Topological domain walls and quantum valley Hall effects in silicene

Youngkuk Kim, Keunsu Choi, and Jisoon Ihm*
Department of Physics and Astronomy, Seoul National University, Seoul 151-747, Republic of Korea

Hosub Jin
Department of Physics and Astronomy, Seoul National University, Seoul 151-747, Republic of Korea
and Center for Functional Interfaces of Correlated Electron Systems, Institute for Basic Science, Seoul National University, Seoul 151-747, Republic of Korea

(Received 21 November 2012; revised manuscript received 9 May 2013; published 28 February 2014)

Silicene is a two-dimensional honeycomb lattice made of silicon atoms, which is considered to be a new Dirac fermion system. Based on first-principles calculations, we examine the possibility of the formation of solitonlike topological domain walls (DWs) in silicene. We show that the DWs between regions of distinct ground states of the buckled geometry should bind electrons when a uniform electric field is applied in the perpendicular direction to the sheet. The topological origin of the electron confinement is demonstrated based on numerical calculations of the valley-specific Hall conductivities, and possible experimental signatures of the quantum valley Hall effects are discussed using simulated scanning tunneling microscopy images. Our results strongly suggest that silicene could be an ideal host for the quantum valley Hall effect, thus providing a pathway to the valleytronics in silicon-based technology.

DOI: 10.1103/PhysRevB.89.085429 PACS number(s): 73.43.−f, 73.20.At, 73.40.−c, 73.22.Pr

I. INTRODUCTION

Recently, silicene, a silicon version of graphene, was successfully synthesized on metal and semiconductor substrates [1–5]. Sharing many intriguing electronic properties with graphene such as Dirac conelike low-energy band structures, silicene has attracted much attention both theoretically and experimentally [6–9]. Moreover, due to its intrinsic buckled geometry [10], diverse phenomena unexpected in graphene have also been suggested. Examples include band gap engineering by an external electric field [6], the quantum spin Hall (QSH) effect [11,12] at experimentally accessible temperature [13], the phase transition from a QSH insulator to a quantum valley Hall (QVH) insulator [14–17] via an external electric field [18–20], and still other exotic topological effects [21–23].

Motivated by the recent synthesis of silicene, here we suggest another interesting topological phenomenon associated with a QVH insulator. A QVH insulator is a topological phase characterized by valley-specific Hall conductivities $\sigma_{\mathrm{H}}^{\mathrm{K}\,(K')}$ and valley-polarized chiral modes emerging on specific sample boundaries [24–26] or domain walls (DWs) [27–33]. In this intriguing topological phase, DWs between regions of different valley Hall conductivities are of particular interest because they may seamlessly glue the momentum space belonging to the same valley, so the DW modes may survive within the midgap region regardless of the crystallographic details of the DWs [34]. Also, it is an exciting idea to host robust conducting channels inside the bulk rather than on edges because they can serve as one-dimensional (1D) conducting wires of circuits integrated in 2D insulators [28,30,31]. The material realization of the topological DWs has been theoretically suggested in bilayer graphene under an inhomogeneous electric field [27,30], in graphene nanoribbon gluing boron nitride sheets [31], and in an AB-BA graphene bilayer tilt boundary under a homogeneous electric field [32,33].

In this paper, we examine a new type of topological DWs based on silicene. We consider the zigzag line interfaces across which the buckling height switches between the two sublattices (Fig. 1), and show that they serve as topological DWs associated with a QVH insulator under a uniform perpendicular electric field. Distinct from the previously suggested topological DWs, the formation of the DWs suggested in this study is assisted by a symmetry-breaking process originated from an intrinsic instability residing in the honeycomb lattice made of silicon atoms. In this respect, the underlying mechanism of the DW formation is more similar to that of solitons in polyacetylene, of which the formation is assisted by the Peierls instability in the 1D metallic chain [35]. Our results based on first-principles calculations confirm that electrons are confined to the DWs when a uniform perpendicular electric field is applied, forming one-dimensional conducting states along the DWs in the otherwise insulating material. The topological origin of the confinement is numerically demonstrated by the direct calculation of the topological invariant associated with the valley-specific Hall conductivities. We also present simulated scanning tunneling microscopy (STM) images to help guide experimental efforts to identify the topological DWs and the QVH effects. Our results suggest that, by introducing the DW in silicene, its electronic and transport properties may be electrically controlled, and therefore, the scope of its applications in the future silicon-based technology can be extended.

II. METHOD

Our first-principles calculations were based on the density-functional theory (DFT). The electronic structure calculation and the structure optimization were performed using the SIESTA package [36] and the VASP code [37], respectively. Exchange and correlation potentials were employed within the local

*jihm@snu.ac.kr

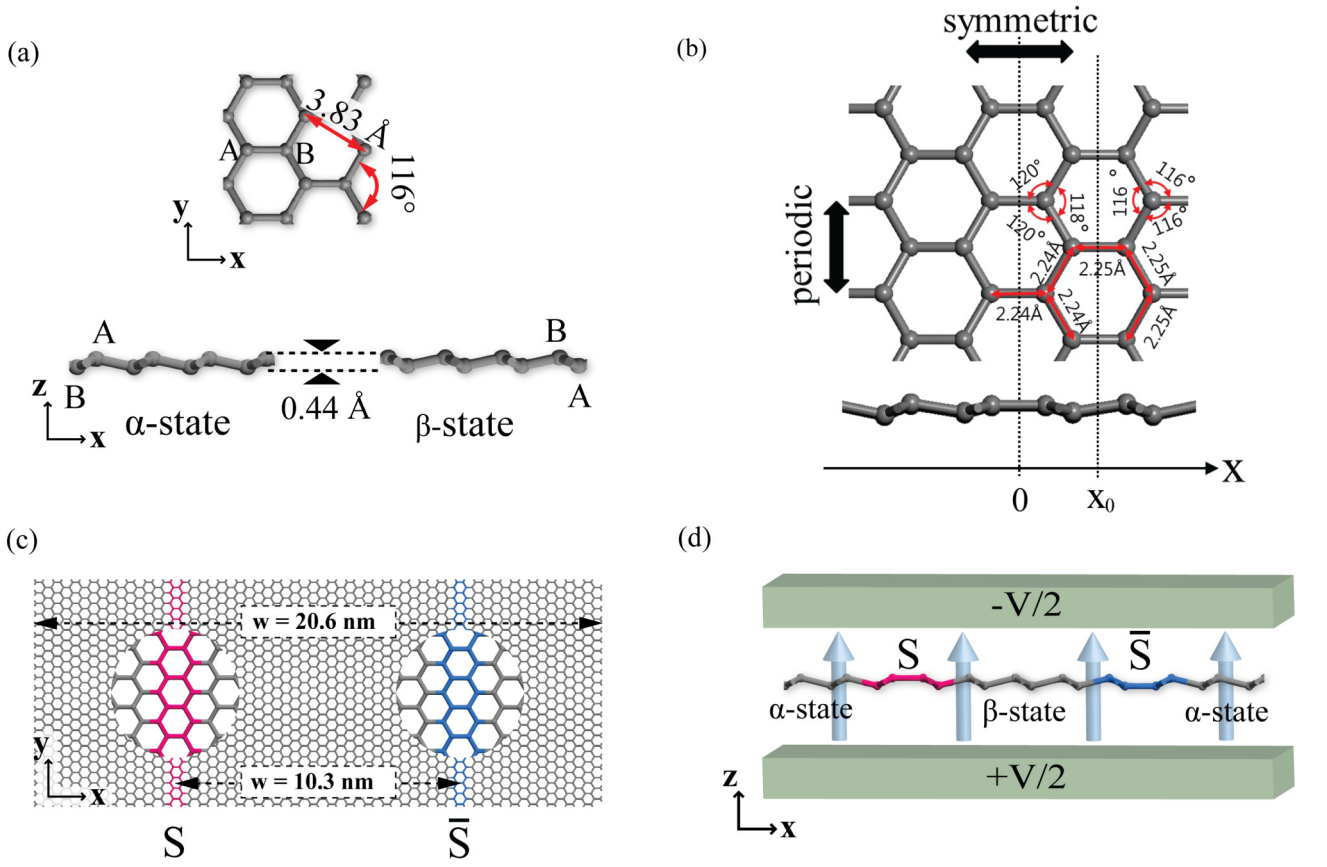

FIG. 1. (Color online) (a) The geometry of the low-buckled silicene. (b) A domain wall (DW) geometry between α and β low-buckled states. (c) Top view of a supercell geometry with zigzag DWs. A pair of solitonlike and antisolitonlike domain walls (S and $\bar{S}$) are separated by 10.3 nm in the supercell. The magnified views of the detailed atomic structure of the S and $\bar{S}$ regions are also illustrated. (d) Schematic configuration of the junction geometry under applied electric fields. The arrows indicate the direction of the applied electric field.

density approximation (LDA) as described by Ceperley and Alder [38]. Periodic sawtooth potentials were introduced to describe the external electric fields. Berry curvatures were calculated on 300×300 numerical grids of the first Brillouin zone (BZ). To circumvent the problems associated with numerical random phases and slow convergence, we adopted the prescription of computing the Berry curvatures on the discretized BZ [39]. Throughout this study we safely ignored the spin degree of freedom because the effect of spin-orbit coupling was negligibly small in the present situation [19,20]. The calculated bond length and the buckling distance were 2.26 Å and 0.44 Å, respectively, as presented in Fig. 1(a).

We constructed a supercell geometry composed of two degenerate buckled geometries [Fig. 1 (a)], and their interfaces were modeled by zigzag lines across which the heights of sublattices were interchanged as shown in Fig. 1(b). In order to fulfill the periodic boundary condition imposed on the supercell, we introduced a pair of DWs denoted by S (soliton) and $\bar{S}$ (antisoliton) in Figs. 1(c) and 1(d). The DWs remained stable upon the full relaxation maintaining the planar geometry under the force criterion of 0.01 eV/Å. The existence of the DWs did not make the junction elbowed or bent during the relaxation. Our total energy calculations of an elbowed geometry, presented in Fig. 2, further confirmed that it cost extra energy to elbow the relaxed planar junction, which should be responsible for the misalignment of perpendicular (p_z) orbitals in forming π or π^* bonding, as in the case of graphene [40]. Another interesting feature of the relaxed geometry was that the structural modifications by the presence of the DWs were confined to a narrow (atomic scale) region near the DWs. As shown in Fig. 1(b), the bond lengths and

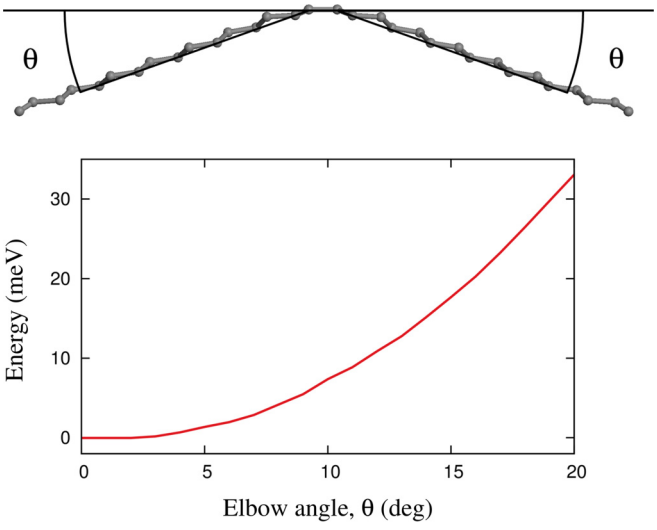

FIG. 2. (Color online) Atomic geometry of the elbowed junction and its total energy curve as a function of the elbow angle θ.

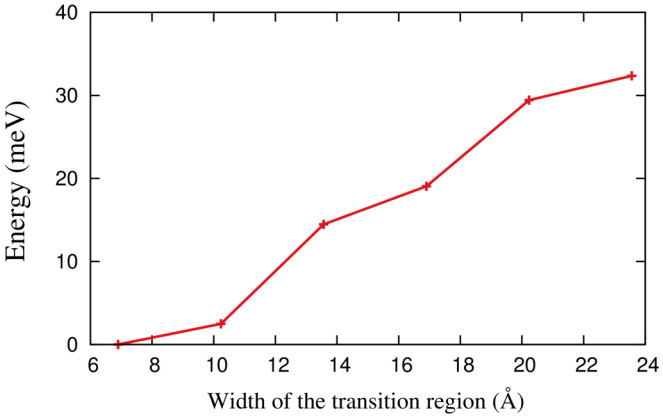

FIG. 3. (Color online) Total energy of the junction geometry as a function of the width of the transition region.

the bond angles at the junction ($x = 0$) were found to be 2.24 Å and 120°, while they were recovered immediately to the bulk values of 2.25 Å and 116° only ∼3 Å away from the DW ($|x| > x_0$). We calculated the formation energies of the junction geometry with a manually widened transition region, and the results showed that the formation energy increased with widening the transition region as presented in Fig. 3. This again confirmed that the system energetically favored the atomic transition to be confined in the narrow region.

III. A CONTINUUM MODEL

Before we present our numerical results, we briefly explain how the buckled geometry of silicene can allow the formation of the topological DWs based on a continuum model. Unlike graphene, free-standing silicene in its perfect planar geometry develops structural instability, which is lifted via so-called low buckling (LB) [10] with one of two sublattices of the honeycomb lattice being shifted (0.44 Å) in the perpendicular direction to the silicene plane. From the LB, the following are expected. (i) The LB spontaneously breaks the reflection symmetry with respect to the silicene sheet (σ_h) developing nonvanishing buckling order parameter (OP), which is defined by the vertical displacement between the two sublattice planes. The symmetry breaking leads to doubly degenerate ground states of the buckled geometry, one of which transforms to the other by reflection [see Fig. 1(a)]. Hereafter, we call them as α and β states, respectively. (ii) Due to the degeneracy, we expect a structural excitation to exist in the form of one-dimensional interfaces separating two vacua ground states, which can be represented by a position-dependent OP $\mu(x)$ asymptotically behaving like a topological soliton (or antisoliton):

$$\lim_{x\to\pm\infty} \mu(x) = \begin{cases} \pm\mu_0 & \text{(soliton)} \\ \mp\mu_0 & \text{(antisoliton)} \end{cases}, \qquad (1)$$

where μ_0 (defined to be positive) and $-\mu_0$ represent the OPs of the two ground buckled geometries (see Fig. 4). In the presence of the electric field E_z, the LB (OP) $\mu(x)$ couples to the field, and gives rise to a position-dependent mass potential $g\mu(x)E_z/v_F^2$ for the Dirac fermions, governed by the effective

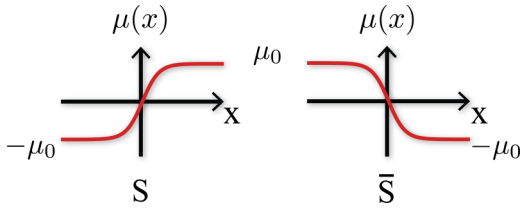

FIG. 4. (Color online) Position-dependent buckling order parameter $\mu(x)$ for soliton (S) and antisoliton ($\bar{S}$).

model Hamiltonian

$$H = \hbar v_F \left(-i\frac{d}{dx}\tau_z\sigma_x + q_y\sigma_y\right) + g\mu(x)E_z\sigma_z. \qquad (2)$$

Here v_F is the Fermi velocity near the Dirac point, and $\boldsymbol{\sigma}$ is the Pauli matrices according to the sublattice index, and $\tau_z = \pm 1$ labels the valley index. $\mathbf{q}$ is the lattice momentum along the parallel direction to the DW and measured from the valley centers at K and K' points. g is introduced to represent the coupling strength (effective charge) between the external field and $\mu(x)$. As noted in the previous work [28], the Hamiltonian supports gapless chiral modes confined to the 1D DW (hereafter, we will call them kink states)

$$\psi_{s,\tau_z}(x,y) \sim e^{iq_y y - s\frac{gE_z}{\hbar v_F}\int_0^x \mu(x')dx'} \begin{pmatrix} 1 \\ -\tau_z i \end{pmatrix}, \qquad (3)$$

with linear energy spectrum $E = -s\tau_z\hbar v_F q_y$ along the DWs. Here $s = \pm 1$ labels a soliton (+1) or an antisoliton (−1). This continuum model explains how the LB allows the formation of the topological DWs. Having established the underlying mechanism, we move to the *ab initio* results confirming the above argument.

IV. RESULTS AND DISCUSSION

Figure 5(a) shows the calculated band structure from the supercell geometry by applying the electric field of 0.5 V/Å. The bulk continuum is represented by the gray shaded area. A bulk band gap of ∼0.1 eV is induced and four branches (ignoring spins) of gapless modes appear in the midgap region. The real-space representation of these states presented in Fig. 5(b) shows that they are localized on DWs and propagating along the parallel direction to the DWs. More specifically, two branches of different valleys and different group velocities are localized one DW, as schematically summarized in Fig. 5(c). Therefore, one branch per spin and per valley emerges on a single DW. This result shows that backscattering is only allowed by changing the valley indices, which guarantees the robustness of valley polarized currents [30] flowing along the 1D metallic DW channels.

Upon varying the strength of the electric field, we find that the degree of localization of electrons to the DWs can be controlled; the electrons are more (less) concentrated on the DWs by increasing (decreasing) the strength of the perpendicular field, as shown in Fig. 6. For example, the probability distribution of b (or equally to c) state, presented in the lower panel of Fig. 6, is more concentrated near the DW ($x = 0$) at $E = 0.5$ V/Å (red curve) than at $E = 0.2$ V/Å (blue curve). This is a natural consequence of the gap size,

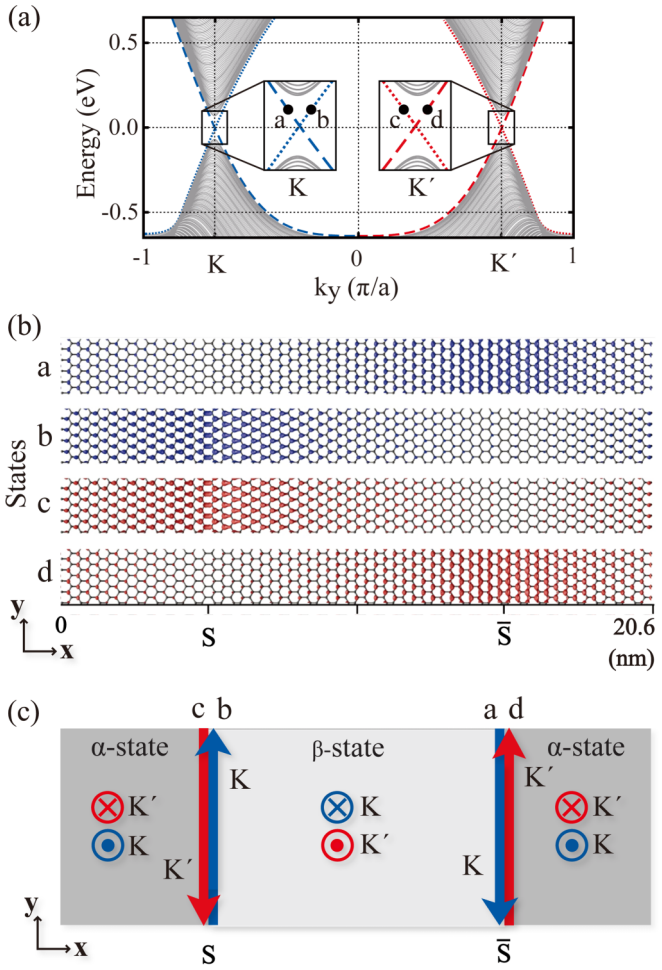

FIG. 5. (Color online) (a) Band structure of the supercell geometry. The solid gray lines in the inset correspond to bulk states, and the dotted and dashed lines indicate the kink states at S and $\bar{S}$, respectively. The blue and red color schemes are used to represent K and K', respectively. The dots (a–d) correspond to the states at 10 meV above the Fermi level. (b) Probability distributions of the QVH kink states at a–d. (c) Schematic illustration of kink states. Electrons at different valleys propagate in opposite directions on the DWs. S supports an upward K current and a downward K' current and vice versa for $\bar{S}$. The senses of the arrows perpendicular to the page represent the sign of the valley Hall conductivities associated with each valley.

which determines the decay length of the kink states [28], being proportional to the strength of the applied field [7]. In the case where $E = 0$ (green curves), the probability distributions become completely delocalized, exhibiting no decaying behavior away from the DW. This behavior reflects the fact that the bulk gap vanishes in the absence of the applied field. Interestingly, we find small but finite localization of the wave functions near the DWs even in the absence of the electric field. As shown in Fig. 7, the probability distribution of b state (or equally to c) at $E = 0$ obtained *with* the DWs (green curve) is slightly localized at the junctions (at $x = 0$ and $x = 10.3$ Å) compared to the probability distribution obtained *without* the DWs (red curve). We attribute this localization behavior to the modification of the atomic structure near the junctions, as discussed in the literature [41]. In their study, it has been

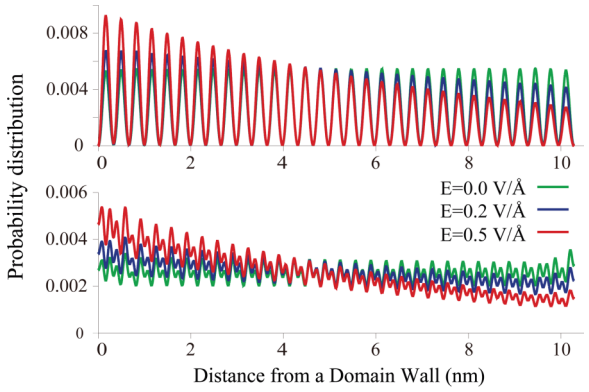

FIG. 6. (Color online) Probability distributions of the wave functions at $E = 10$ meV from the Fermi energy. The top panel corresponds to a (or equally to d) state, and the bottom panel corresponds to b (or equally to c) state in Fig. 5(a). By increasing the applied electric field, states become more concentrated on the DW.

shown that the coupling of the junction atoms to the rest of the system can be written as $-t(1 + e^{\pm ik_y a})$, where $t = 1.1$ eV is the hopping parameter. The corresponding k_y values for b and c states are $(-2/3 + 0.004)\pi/a$ and $(2/3 - 0.004)\pi/a$, respectively. At these values, the effective couplings become slightly intensified, thereby resulting in the localization of the electrons to the DWs.

Although we only present the results obtained from a particular atomic configuration of DWs as a representative example, we have tested different atomic configurations of DWs, and always found two midgap branches per spin on a single DW. Depending on the crystallographic details, the DWs may produce an interaction mixing two valleys, thus leading to the opening of a subgap in the kink-states band. We actually have found several configurations inducing the armchair DWs that open a subgap, and its size has been typically ∼1 meV. Since the subgap size is much smaller than the bulk gap (∼0.1 eV), the kink states remain in the bulk gap region, determining the low-energy transport properties. In fact, this result has a topological origin; the number of kink

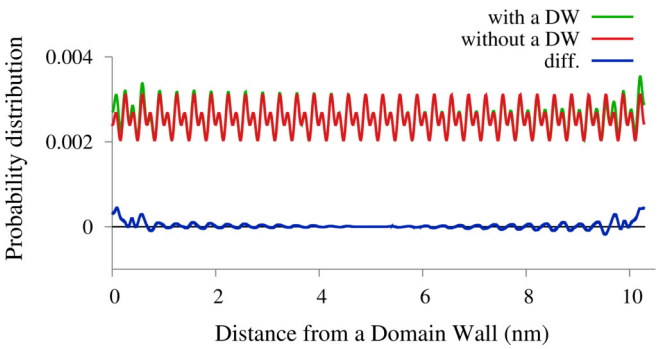

FIG. 7. (Color online) Changes in the probability distribution near a domain wall. The green and red (overlapped) curves represent probability distributions obtained with and without the DW, respectively, in the absence of the applied electric field. The blue (lower) curve represents the changes in the probability distributions due to the DW.

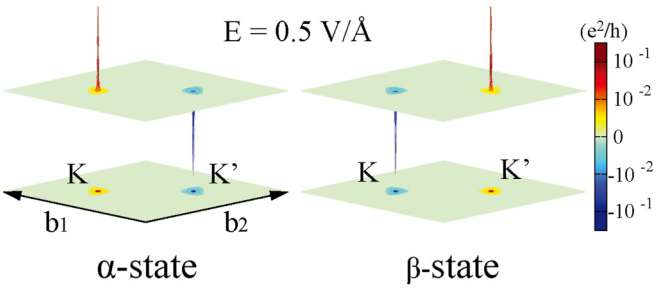

FIG. 8. (Color online) Berry curvatures for the α state (left panel) and the β state (right panel) under the applied electric field of 0.5 V/Å using the color code scale in units of e^2/h.

states emerging on the DW is determined by the topological invariant, defined to be the difference between the valley Hall conductivities in the adjacent bulk (i.e., infinitely extended in two dimensions) domains [29,34,42]. To further discuss this point, we numerically calculate Berry curvatures and valley Hall conductivities [14]. The left panel of Fig. 8 shows the Berry curvature obtained from the α state of the buckled geometry under the electric field of 0.5 V/Å. Note that Berry curvatures are highly concentrated on the K and K' points having opposite signs in different valleys. The valley Hall conductivities are obtained by integrating the Berry curvatures on the BZ [17]. We note that two valley indices share the same BZ, and therefore, in general, there exists intrinsic ambiguity in assigning the portions of the BZ to calculate a specific valley Hall conductivities [34]. Therefore, in some largely gapped system, numerical calculations beyond the $\mathbf{k}\cdot\mathbf{p}$ description may result in unquantized valley Hall conductivities. Nonetheless, in the present system, the valley Hall conductivities are accurately defined because the Berry curvatures are well concentrated in the vicinity of valley centers (K and K') points. Our numerical results show that, upon the integration of the Berry curvature up to $\sim$0.5 Å^{-1} from the K (K') point, the valley Hall conductivity is fully converged to 1/2 ($-1/2$) in units of $2e^2$/h (the factor 2 accounts for spins), resulting in $\sigma_{\mathrm{H}}^{K\,(K')} = +(-)1/2$. This result confirms the QVH insulating state introduced in the low-buckled silicene by an applied electric field. Also, the integration of the Berry curvature over the whole BZ gives zero, which reconfirms the fact that the (charge) Hall conductivity should vanish in a time-reversal invariant band insulator.

The α state of the buckled geometry is obtained by the C_2 rotation of the β state around the z axis, which exchanges the valley indices between K and K'. Therefore, the K (K') point of the α state plays the role of the K' (K) point in the β state. This feature is reflected in our numerical calculations of the Berry curvatures as shown in Fig. 8, i.e., $\sigma_{\mathrm{H},\alpha}^{K(K')} = -\sigma_{\mathrm{H},\beta}^{\mathrm{K}(K')}$, where $\sigma_{\mathrm{H},\alpha(\beta)}^{K(K')}$ is the valley Hall conductivity calculated in the α (β) state for a given valley index K (K'). The two buckled ground states host different QVH states under a uniform electric field characterized by different valley Hall conductivities. The result is consistent with the chiral asymmetric index theorem [42], which dictates that the number of the kink states emerging on a single DW is determined by a topological invariant defined to be the difference of the valley Hall conductivities (in unit of $2e^2/h$) between adjacent domains, $\sigma_{\mathrm{H},\alpha}^{K\,(K')} - \sigma_{\mathrm{H},\beta}^{\mathrm{K}\,(K')}$. Note that we have obtained the valley Hall conductivities of $\pm 1/2$ for two buckled states, thus $\sigma_{\mathrm{H};\alpha}^{K\,(K')} - \sigma_{\mathrm{H};\beta}^{K\,(K')} = 1(-1)$ in good agreement with the number of kink states emerging on a DW per valley. The sign indicates the propagating direction of the chiral kink states. This result explains the topological origin of the kink states, which can protect the number of DW modes regardless of the crystallographic configuration of the DW [34]. In practice, however, we may have to pay more attention to zigzag-line-like DWs than others, because they are more easily produced according to our formation energy calculations. We find that the formation energy of the zigzag DWs is $\sim$25 meV/Å, which is smaller than that of other tested configurations such as armchair DWs with the formation energy of $\sim$39 meV/Å.

Finally, we propose a way of detecting the formation of DWs as well as the QVH effects in silicene by using STM. Figures 9(a) and 9(b) simulate the STM images under the sample bias V_{bias} of -20 mV, and Figs. 9(c) and 9(d) simulate $V_{\mathrm{bias}} = -1.4$ V. Figures 9(a) and 9(c) correspond to the states localized at S, while Figs. 9(b) and 9(d) correspond to those at $\bar{\mathrm{S}}$. Bright protrusions in the STM images show the upper-buckled silicon atoms forming the triangular lattice in each domain. The DWs can readily be identified as the lines shifting the locations of protrusions from one sublattice to the other as shown in the middle of the images. The simulated images in Figs. 9(c) and 9(d) represent the filled states in the energy window from the Fermi energy to -1.4 eV, where extended bulk states make major contributions and thus exhibit almost no change as the applied electric field varies. However, the simulated STM images under a sample bias of -20 mV and applied external field of 0.5 V/Å [Figs. 9(a) and 9(b)] show a noticeable change by the applied field. These figures represent the filled kink states residing in the bulk gap. Comparing with the simulated STM images at $V_{\mathrm{bias}} = -1.4$ V [Figs. 9(c) and 9(d)], the brightness of the protrusion is

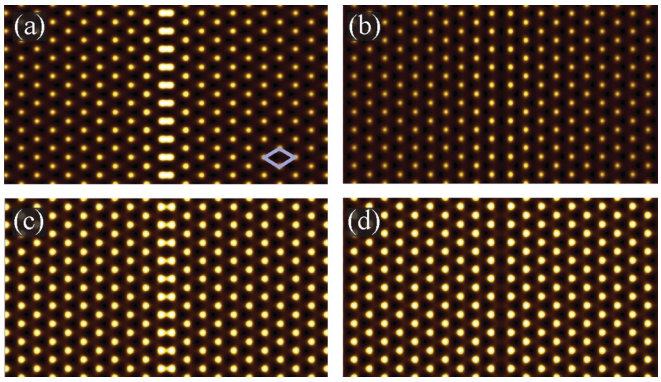

FIG. 9. (Color online) (a)–(d) Simulated scanning tunneling microscopy (STM) images for soliton [(a) and (c)] and antisoliton [(b) and (d)] DWs at different sample biases. The rhombus in (a) represents the 1 × 1 unit cell. Sample biases are chosen to be -20 mV in (a) and (b), and -1.4 V in (c) and (d). An external field of 0.5 V/Å is applied perpendicular to the sheet in (a) and (b). Bright spots correspond to the upper buckled silicon atoms, and DWs reside along the center of the images.

attenuated away from the DWs in Figs. 9(a) and 9(b), which reflects the kink states being localized on the topological DWs and exponentially decaying in the asymptotic region [27]. For the small bias of −20 mV, reducing (turning off) the applied electric field leads to the reduction (disappearance) of the attenuation, and the simulated images resemble those of $V_{bias} = -1.4$ V. Therefore, STM images under varying electric fields are signatures of the QVH effect in silicene, and STM should be useful for identifying the DWs and the associated kink states, thus providing direct evidence for the QVH effect.

V. SUMMARY

In summary, we have presented a first-principles study on the QVH effects in silicene. The buckled geometry of silicene allows the manifestation of the QVH effects through DWs. Electrons are confined to the DWs by applying a perpendicular electric field, forming gapless kink states. The kink states exhibit common features of the QVH chiral states such as the valley polarization, valley Hall currents propagating oppositely for different valley indices, and the absence of backscattering. In particular, we have provided the first-principles confirmation of the chiral asymmetric index theorem [34,42], which guarantees the number of kink states emerging on the DWs. We have also provided simulated STM images to show that STM experiments can directly observe the QVH effects in silicene. Our results suggest that the DWs may serve as robust conducting wires embedded in silicene and enable the realization of valleytronics [43] as a next-generation electronics in the silicon-based industry.

ACKNOWLEDGMENTS

This work was supported by the National Research Foundation (NRF) of Korea through MEST Basic Research No. 2006-0093853, the 2010 Korea-Sweden Research Cooperation Program of NRF, and the Core Competence Enhancement Program of Korea Institute of Science and Technology. The computations were performed via the support of Korea Institute of Science and Technology Information. Y.K. greatly appreciates J. Jung, E. G. Moon, and J. Im for fruitful discussions and comments.

[1] P. Vogt, P. De Padova, C. Quaresima, J. Avila, E. Frantzeskakis, M. C. Asensio, A. Resta, B. Ealet, and G. Le Lay, Phys. Rev. Lett. **108**, 155501 (2012).
[2] B. Lalmi, H. Oughaddou, H. Enriquez, A. Kara, S. Vizzini, B. Ealet, and B. Aufray, Appl. Phys. Lett. **97**, 223109 (2010).
[3] B. Feng, Z. Ding, S. Meng, Y. Yao, X. He, P. Cheng, L. Chen, and K. Wu, Nano Lett. **12**, 3507 (2012).
[4] A. Fleurence, R. Friedlein, T. Ozaki, H. Kawai, Y. Wang, and Y. Yamada-Takamura, Phys. Rev. Lett. **108**, 245501 (2012).
[5] L. Chen, C.-C. Liu, B. Feng, X. He, P. Cheng, Z. Ding, S. Meng, Y. Yao, and K. Wu, Phys. Rev. Lett. **109**, 056804 (2012).
[6] Z. Ni, Q. Liu, K. Tang, J. Zheng, J. Zhou, R. Qin, Z. Gao, D. Yu, and J. Lu, Nano Lett. **12**, 113 (2012).
[7] N. D. Drummond, V. Zólyomi, and V. I. Fal'ko, Phys. Rev. B **85**, 075423 (2012).
[8] A. Kara, H. Enriquez, A. P. Seitsonen, L. L. Y. Voon, S. Vizzini, B. Aufray, and H. Oughaddou, Surf. Sci. Rep. **67**, 1 (2012).
[9] P. De Padova, O. Kubo, B. Olivieri, C. Quaresima, T. Nakayama, M. Aono, and G. Le Lay, Nano Lett. **12**, 5500 (2012).
[10] S. Cahangirov, M. Topsakal, E. Aktürk, H. Şahin, and S. Ciraci, Phys. Rev. Lett. **102**, 236804 (2009).
[11] C. L. Kane and E. J. Mele, Phys. Rev. Lett. **95**, 226801 (2005).
[12] B. A. Bernevig, T. L. Hughes, and S.-C. Zhang, Science **314**, 1757 (2006).
[13] C.-C. Liu, W. Feng, and Y. Yao, Phys. Rev. Lett. **107**, 076802 (2011).
[14] D. Xiao, W. Yao, and Q. Niu, Phys. Rev. Lett. **99**, 236809 (2007).
[15] F. Zhang, J. Jung, G. A. Fiete, Q. Niu, and A. H. MacDonald, Phys. Rev. Lett. **106**, 156801 (2011).
[16] W. Yao, S. A. Yang, and Q. Niu, Phys. Rev. Lett. **102**, 096801 (2009).
[17] W. Yao, D. Xiao, and Q. Niu, Phys. Rev. B **77**, 235406 (2008).
[18] M. Ezawa, New J. Phys. **14**, 033003 (2012).
[19] M. Ezawa, Phys. Rev. B **86**, 161407 (2012).
[20] M. Tahir and U. Schwingenschlögl, Sci. Rep. **3**, 03192 (2013).
[21] M. Ezawa, Phys. Rev. Lett. **109**, 055502 (2012).
[22] A. R. Wright, Sci. Rep. **3**, 02736 (2013).
[23] M. Ezawa, Phys. Rev. Lett. **110**, 026603 (2013).
[24] E. V. Castro, N. M. R. Peres, J. M. B. Lopes dos Santos, A. H. Castro Neto, and F. Guinea, Phys. Rev. Lett. **100**, 026802 (2008).
[25] X. Li, Z. Qiao, J. Jung, and Q. Niu, Phys. Rev. B **85**, 201404 (2012).
[26] J. Li, I. Martin, M. Buttiker, and A. F. Morpurgo, Nature Phys. **7**, 38 (2011).
[27] I. Martin, Y. M. Blanter, and A. F. Morpurgo, Phys. Rev. Lett. **100**, 036804 (2008).
[28] G. W. Semenoff, V. Semenoff, and F. Zhou, Phys. Rev. Lett. **101**, 087204 (2008).
[29] J. Jung, F. Zhang, Z. Qiao, and A. H. MacDonald, Phys. Rev. B **84**, 075418 (2011).
[30] Z. Qiao, J. Jung, Q. Niu, and A. H. MacDonald, Nano Lett. **11**, 3453 (2011).
[31] J. Jung, Z. Qiao, Q. Niu, and A. H. MacDonald, Nano Lett. **12**, 2936 (2012).
[32] A. Vaezi, Y. Liang, D. H. Ngai, L. Yang, and E.-A. Kim, Phys. Rev. X **3**, 021018 (2013).
[33] F. Zhang, A. H. MacDonald, and E. J. Mele, Proc. Natl. Acad. Sci. USA **110**, 10546 (2013).
[34] J. Li, I. Martin, M. Büttiker, and A. F. Morpurgo, Phys. Scr. **2012**, 014021 (2012).
[35] W. P. Su, J. R. Schrieffer, and A. J. Heeger, Phys. Rev. Lett. **42**, 1698 (1979).
[36] J. M. Soler, E. Artacho, J. D. Gale, A. García, J. Junquera, P. Ordejón, and D. Sánchez-Portal, J. Phys.: Condens. Matter **14**, 2745 (2002).
[37] G. Kresse and J. Furthmüller, Phys. Rev. B **54**, 11169 (1996).

[38] D. M. Ceperley and B. J. Alder, Phys. Rev. Lett. **45**, 566 (1980).

[39] T. Fukui, Y. Hatsugai, and H. Suzuki, J. Phys. Soc. Jpn. **74**, 1674 (2005).

[40] D.-B. Zhang, E. Akatyeva, and T. Dumitrica, Phys. Rev. Lett. **106**, 255503 (2011).

[41] M. P. Lima, A. Fazzio, and A. J. R. da Silva, Phys. Rev. B **88**, 235413 (2013).

[42] G. E. Volovik, *The Universe in a Helium Droplet* (Oxford University Press, New York, 2003).

[43] D. Gunlycke and C. T. White, Phys. Rev. Lett. **106**, 136806 (2011).